Macromolecules

ARTICLE

pubs.acs.org/Macromolecules

Rheology and SANS on PET-*b*-PLAc-*b*-P(DMAEMAq) Triblock Copolymers: Impact of the PET and Polyelectrolyte Chain Length

Livie Liénafa,[†] Julian Oberdisse,[*,‡,⊥] Serge Mora,[§] Sophie Monge,[*,†] and Jean-Jacques Robin[†]

[†]Institut Charles Gerhardt Montpellier UMR5253 CNRS-UM2-ENSCM-UM1, Equipe Ingénierie et Architectures Macromoléculaires, Université Montpellier II, Bat 17, cc1702, Place Eugène Bataillon 34095 Montpellier Cedex 5, France

[‡]Laboratoire Charles Coulomb UMR 5221, CNRS, 34095, Montpellier, France

[§]Laboratoire Charles Coulomb UMR 5221, Université Montpellier 2, 34095, Montpellier, France

[⊥]Laboratoire Léon Brillouin UMR 12 CNRS/CEA, CEA Saclay, 91191 Gif-sur-Yvette, France

Supporting Information

ABSTRACT: We report on a small angle neutron scattering (SANS) study of self-organization of a novel triblock copolymer containing a crystalline poly(ethylene terephthalate) oligomer, a rubbery poly(lauryl acrylate) midblock, and a polyelectrolyte block (quaternized poly(2-(dimethylamino)ethyl methacrylate)) of various length. The rheology of the solutions showed a transition from Newtonian flow at low concentrations, to shear-thinning at intermediate concentrations, and finally a yield behavior at high concentrations. The microstructure of the samples investigated by SANS was found to evolve strongly with the polyelectrolyte block length. The data were analyzed in terms of aggregation numbers, radius of gyration, and aggregate hydration. Complete modeling of the intensity curves was achieved by an inversion method extracting an average aggregate radial volume fraction profile. In both rheology and microstructure, a surprising strong impact of the small PET block was observed.

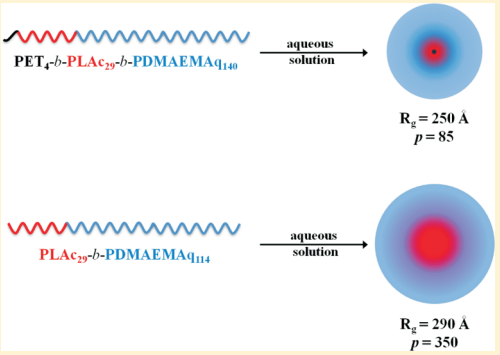

1. INTRODUCTION

Amphiphilic block copolymers have attracted considerable attention due to their ability to self-assemble in selective solvents.[1−6] In aqueous solution, micelles consisting of a hydrophobic core surrounded by a shell of the solvated hydrophilic part of the block copolymer can be formed, as with simple surfactants. Moreover, due to the wealth of accessible conformations, amphiphilic macromolecules can aggregate into various microstructures. For example, a polyelectrolyte block can not only adopt different conformations depending on ionic strength, but also induce repulsive interactions between aggregates in solution even at low nominal concentrations.[7−11] This leads to a significant increase in viscosity of the solutions, possibly changing their nature from purely viscous to highly elastic or yielding. Another interesting case is found with telechelic copolymers, e.g., copolymers having two hydrophobic stickers.[12] At high enough concentrations, such molecules induce the formation of a physical network due to attractive interactions between micelles.[13] Generally, the rheological behavior of these systems thus depends on the volume fraction Φ of polymers in solution.

The triblock copolymers studied in this contribution have an additional original feature, a short poly(ethylene terephthalate) (PET) oligomer. PET is a frequently used industrial polymer, with important applications for fibers and packaging, in particular due to its transparency, mechanical strength and chemical resistance. Its high consumption makes PET recycling an important issue.[14] Chemical recycling consists in the PET depolymerization, which produces oligomers or monomers.[14,15] These products can be used as chemical intermediates for the production of new materials, and such oligomers have been synthesized as starting point for the present study. The second block of the hydrophobic segment is poly(lauryl acrylate) (PLAc). PET oligomers are semicrystalline polymers with relatively high glass transition temperature (Tg) whereas PLAc possesses a low T_g value. Moreover, due to the difference in behavior of crystalline PET and rubbery PLAc at room temperature, these two polymers are not miscible, and interesting new physics of the self-assembly of the hydrophobic core can be expected. This is similar to mixtures of hydrocarbon and fluorocarbon chains of copolymers and surfactants.[13,16] The hydrophilic block is a polyelectrolyte, the poly(2-(dimethylamino)ethyl methacrylate) (PDMAEMA) quaternized with methyl iodide. Since quaternization of the amine groups in the PDMAEMA component yields a strong cationic polyelectrolyte PDMAEMAq, the hydrophilic character of the copolymer and its solubility in water is improved.[7]

A series of triblock copolymers based on PLAc and PDMAEMA were prepared by atom transfer radical polymerization

Received: February 12, 2011
Revised: May 24, 2011
Published: June 07, 2011

Scheme 1. Chemical Structures of the Four Block Copolymers Used in This Study

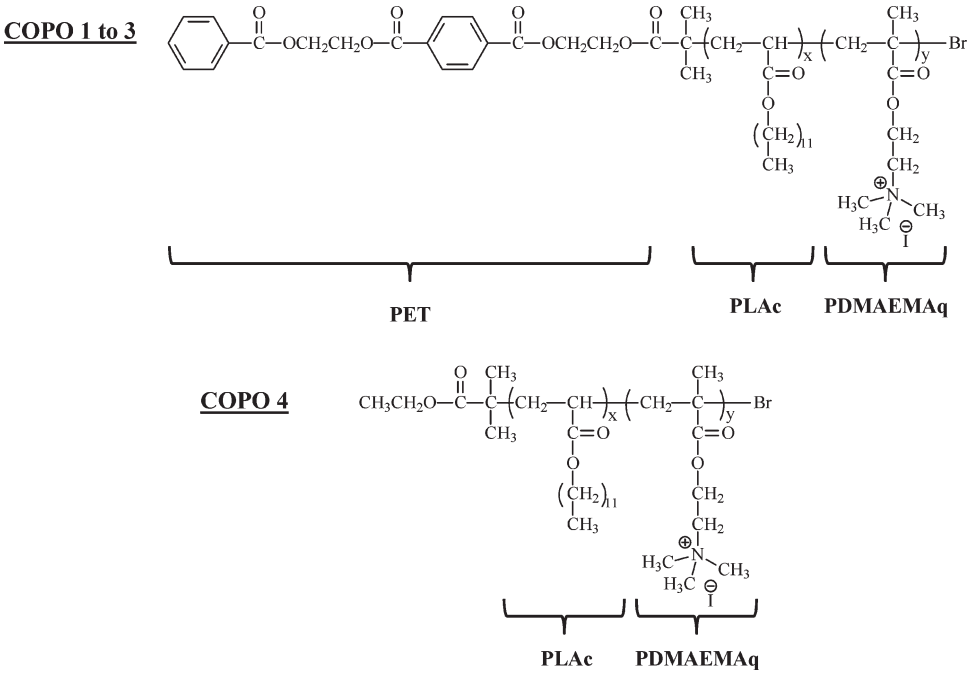

Table 1. Copolymer Molecular Characteristics: Number Average Molecular Weights of the Polyelectrolyte Block and of the Copolymer, Molecular Volumes, and Difference in Scattering Length Density between the Polymer and the Solvent[a]

	block copolymers					
		$M_{PDMAEMAq}$ (g mol^{-1})	M_i[b] (g mol^{-1})	PDI[c]	V_i (cm^3)	$\Delta\rho_i$[b] (cm^{-2})
COPO 1	PET_4-*b*-$PLAc_{29}$-*b*-$PDMAEMAq_{45}$	7700	15200	1.38	2.8×10^{-20}	6×10^{10}
COPO 2	PET_4-*b*-$PLAc_{29}$-*b*-$PDMAEMAq_{77}$	13200	20700	1.30	3.7×10^{-20}	6×10^{10}
COPO 3	PET_4-*b*-$PLAc_{29}$-*b*-$PDMAEMAq_{140}$	24000	31500	1.32	5.7×10^{-20}	6×10^{10}
COPO 4	$PLAc_{29}$-*b*-$PDMAEMAq_{114}$	19600	26600	1.30	4.8×10^{-20}	6×10^{10}

[a] M_{PET} = 500 g·mol^{-1}, M_{LAc} = 7000 g·mol^{-1}. *M* values were determined using ^{1}H NMR spectra. $\Delta\rho_i = \rho_{solvent} - \rho_i$ with $\rho_i = 0.4 \times 10^{10}$ cm^{-2} and $\rho_{solvent} = 6.4 \times 10^{10}$ cm^{-2}. [b] Determined by ^{1}H NMR. [c] Determined by size exclusion chromatography using THF as eluent (1 mL/min) and PS calibration ***before quaternization.*** PDI of PET_4-*b*-PLAc was 1.17.

(ATRP) using the PET block as macroinitiator.[17] These novel block copolymers may be attractive for diverse applications such as drug delivery, coatings, and colloids stabilization. Their structure depends on the nature and molecular weights of the blocks, solvent interactions, and the architecture of the block copolymer.[7,18]

In this article, we have studied the rheological behavior and structure of different triblock copolymers in aqueous solution. In particular, we have focused on the influence of the PDMAEMAq block molecular weight, as well as that of the PET block. To our knowledge, it is the first time that the influence of the polyethylene terephthalate on the self-assembly of block copolymers was reported in the literature. The obtained results are important as they open the way to the use of recycled PET oligomers for purposes implying structuring and modifications of dynamics. Small-angle neutron scattering (SANS) was performed to investigate the relationship between microstructure of the aggregates and the rheological behavior. SANS data were first analyzed with standard methods and then using a model specially developed for core−shell structures.

2. METHODS: EXPERIMENTAL AND MODELING

2.1. Sample Preparation. Different polymers were prepared: three triblock (poly(ethylene terephthalate)-*block*-poly(lauryl acrylate)-*block*-quaternized poly(2-(dimethylamino)ethyl methacrylate)) (PET-*b*-PLAc-*b*-PDMAEMAq) and one diblock copolymer (poly(lauryl acrylate)-*block*-quaternized poly(2-(dimethylamino)ethyl methacrylate)) (PLAc-*b*-PDMAEMAq), as shown in Scheme 1. The triblocks (COPO 1 to 3) differ by the mass of the hydrophilic block, whereas the diblock (COPO 4) lacks the PET block.

All materials were synthesized by atom transfer radical polymerization (ATRP) in two steps (Supporting Information): (i) the polymerization of lauryl acrylate from PET macroinitiator or ethyl-2-bromoisobutyrate and (ii) the polymerization of the 2-(dimethylamino)ethyl methacrylate followed by permethylation with methyl iodide. Details of the synthesis

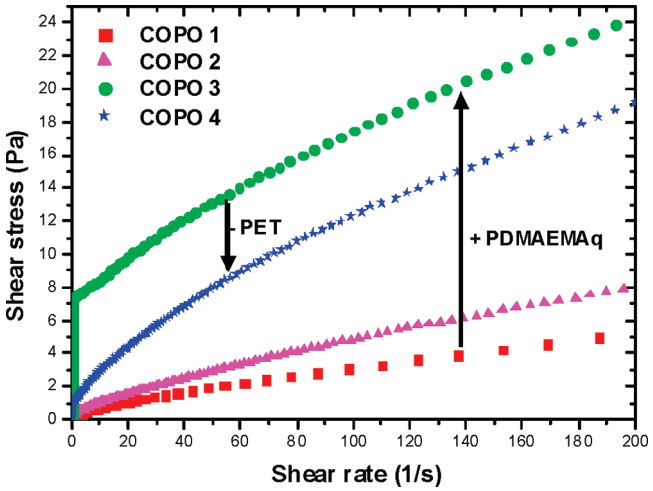

Figure 1. Evolution of shear stress with shear rate (measured by dynamic experiments where the stress was ramped from 0 to 25 Pa) for COPO 1 to 4 at Φ = 3.6%. COPO 1 to 3 are triblock copolymers with PET with increasing polyelectrolyte block length (PDMAEMAq 8k, 13k, 24k), COPO4 is a diblock copolymer (PDMAEMAq 20k), without PET.

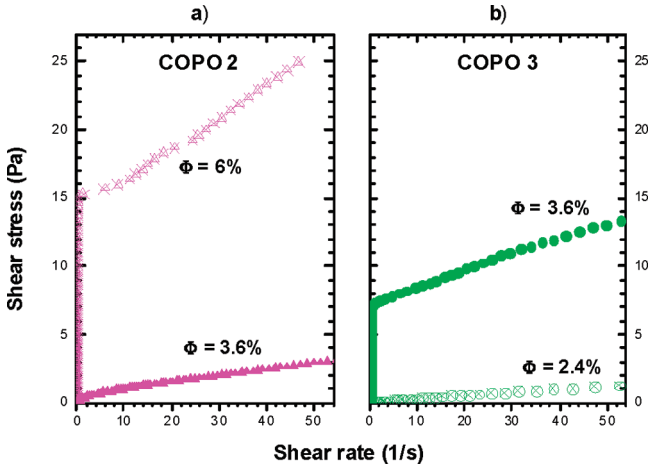

Figure 2. Evolution of shear stress with shear rate measured by dynamic experiments where the stress was ramped (from 0 to 25 Pa) (a) for COPO 2 at Φ = 3.6 and 6% and (b) for COPO 3 at Φ = 2.4 and 3.6%.

and characterization of these copolymers will be described in a forthcoming publication.[19] Polymerizations were carried out using Schlenk line and syringe techniques under nitrogen. Polymer conversions were determined by ^{1}H NMR spectra (δ, ppm) recorded on a Bruker DRX 300 MHz spectrometer. Molecular weights and molecular weights distributions were determined through size exclusion chromatography (SEC) with a system equipped with a Water 2410 refractive index detector and PLgel columns. THF was used as the mobile phase at a flow rate of 1 mL.min^{-1} at 25 °C. Monodispersed polystyrene standards (Polymer Laboratories) were used to generate the calibration curve. The main characteristics of the triblock copolymers are gathered in Table 1. As the molecular weight distributions, determined before the quaternization step, were close for all copolymers, we assumed that this parameter did not influence the aggregation behavior.

2.2. Small Angle Neutron Scattering (SANS). SANS measurements were carried out at Laboratoire Léon Brillouin (Saclay, France). The data were collected on instrument PACE. Three configurations (sample-to-detector distance, incident neutron wavelength) were used: 1 m at 6 Å and 4.5 m at 6 and 12 Å, covering a q-range from 0.003 to 0.3 Å^{-1}. The samples were prepared in pure D_2O. Empty cell scattering has been subtracted and detector efficiency has been corrected with 1 mm H_2O scattering. All measurements were carried out at 25 °C and 2 mm light path Hellma quartz cells were used. Data were normalized to obtain absolute units (cm^{-1}) by an independent measurement of the incoming flux. For simplicity, the resulting scattering cross section per unit volume $(d\Sigma)/(d\Omega)|_V$ is called $I(q)$ here. The incoherent background was estimated with H_2O/D_2O mixtures. The excess scattering length density ($\Delta\rho$) of aggregates with respect to D_2O, reported in Table 1, were calculated from data established by Sears[20] and the molecular volumes estimated from the monomer density (Supporting Information).

2.3. Modeling of SANS Data. A classical way of analyzing small angle scattering data of dilute aggregated objects in solution is to check first that only form factor information is measured by superimposing I/Φ, where Φ denotes the polymer volume fraction. One can then extract the average aggregation number from the low-q limit of the intensity I_0. The typical size of the aggregates can be deduced from the radius of gyration, and some information on average conformation is given by high-q data. For other copolymers, we have deduced an estimate of the typical hydration of each aggregate from the combination of the aggregation number and the typical dimensions.[21−23] We now present a more detailed analysis based on a multishell modeling of the monomer density profile of average aggregates. In this approach, the connectivity of the chain molecules is explicitly discarded.[24]

In our model, it is assumed that the monomers, the average number of which was deduced from I_0, were distributed over concentric spherical shells of thickness Δr. The maximum shell radius R_{max} was taken as two times the experimental radius of gyration, without any impact on the resulting profile which vanished above $1.5R_g$. The intrinsic problem of such a model was that the number of parameters—given by the monomer volume fractions in each shell—was greater than the amount of information actually contained in the scattering curve. The solution for this ill-posed problem was conceptually close to the indirect Fourier transform.[25] It consisted in searching profiles $\Phi(r)$ which did not only optimize the agreement with the experimental curve $I(q)$, but also contained a minimum amount of spurious information. In practice, this was achieved by simultaneously optimizing the agreement between the model prediction $I_{mod}(q)$ calculated from the radial volume fraction profile $\Phi(r)$ and the experimental result $I(q)$ via χ^2, which is a measure of the discrepancy between the experimental and the modeled intensity values

$$\chi^2 = \frac{1}{N_q}\sum_{i=1}^{N_q}\left(\frac{I(q_i) - I_{mod}(q_i)}{\Delta I}\right)^2 \quad (1)$$

and a parameter characterizing the smoothness of the profile

$$k^2 = \frac{1}{N_p - 1}\sum_{i=1}^{N_p - 1}(\Phi_{i+1} - \Phi_i)^2 \quad (2)$$

In eqs 1 and 2, N_q denoted the number of intensity data points, N_p the number of points in the volume fraction profile, and ΔI the possibly q-dependent error bar on the experimental intensity. The radial volume fraction profile $\Phi(r)$ was approximated as a discrete set of points Φ_i, one for each shell. The simultaneous minimization of χ^2 and k^2 was done by minimizing the sum

$$\chi^2 + \lambda k^2 \quad (3)$$

using a random motion of the monomers from one shell to another as Monte Carlo steps, coupled to a simulated annealing procedure.[26,27] In eq 3, λ was the stability parameter (commonly called Lagrange multiplier) to be found. The stability plot analysis was performed by screening values of χ^2 and k^2 for different λ, and identifying the point where the constraint on smoothness decreased the quality of the fit (χ^2). An example of the stability plot and parameters of the model such as shell

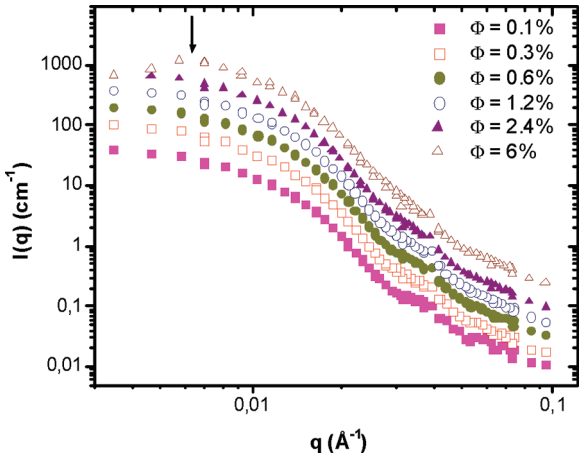

Figure 3. Structure of aqueous solutions of COPO 2. Scattered intensities $I(q)$ as a function of wave vector q are plotted for different volume fractions Φ ranging from 0.1 to 6%.

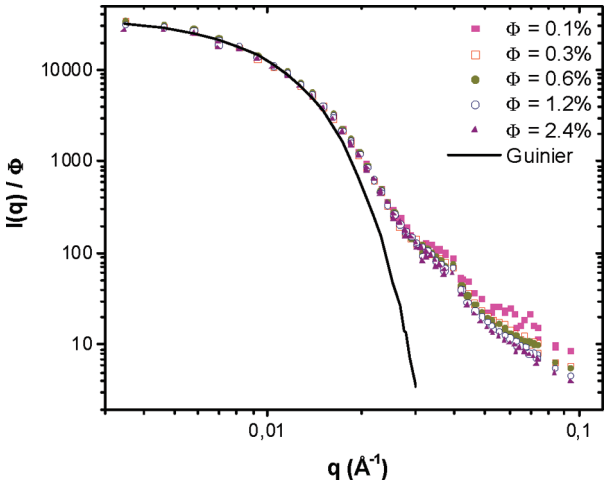

Figure 4. Scattered intensity $I(q)$ (in cm^{-1}) normalized by the volume fraction from aqueous solutions of COPO 2 for Φ = 0.1 to 2.4%. The solid line is the Guinier approximation valid at small q.

thickness, maximum shell radius, and molecular volumes were given in the Supporting Information. Because of the absence of any description of chain connectivity, and to the finite Δr, the model was expected to break down in the high-q range.

2.4. Rheology. Measurements were carried out at 25 °C using a stress-controlled rheometer Physica UDS 200 with Couette geometry (inner radius = 12.5 mm, gap = 1.06 mm). Two different kinds of experiment were achieved: (i) creep experiment and (ii) dynamic experiment. In the first one, a given stress was held constant and the strain rate was measured as a function of time. In both cases, the sample was sheared at 25 Pa during 5 min and then it was left at rest (stress equal to zero) for 24 h. In dynamic experiment, the stress was increased from 0.1 to 25 Pa with a logarithmic ramp. Copolymer solutions were prepared by vigorous dispersion for 1 h in deionized water. After complete dissolution, gels were stored at 4 °C and were analyzed 3 days after their preparation.

3. RESULTS

3.1. Rheology. The rheological behavior of solutions of amphiphilic copolymers considered in this study was investigated using dynamic (stress ramp) and creep experiments. Aqueous solutions of COPO 1 to 4 with polymer volume fraction Φ comprising between 1.2 and 6% have been prepared. We have observed that: (i) the rheological nature of the solutions changed with concentration, higher concentrations leading to very viscous solutions, and that (ii) a transient flow behavior was observed during a creep test before the shear rate reached a steady-state value, which was zero if the applied stress was below the yield stress.

COPO 1 to 3 differ only in their hydrophilic (PDMAEMAq) block length: the one of COPO 2 is two times longer than the one of COPO 1, and the one of COPO 3 three times. The flow curves of these three copolymers at Φ = 3.6% were compared (Figure 1). The hydrophilic block length was immediately seen to have an influence on the rheological behavior of the copolymer solutions. The longer the PDMAEMAq block, the higher the stress at a given shear rate, with a marked increase when going from COPO 2 to COPO 3. The influence of the PET block was evidenced by superimposing the stress of the diblock copolymer without the PET block (called COPO 4) to the other triblock copolymers, which included its analogue, COPO 3. The stress is slightly lower, indicating that the missing PET block affected the structure of the solution. An important feature of Figure 1 is that the growth of a yield stress was clearly visible. For COPO 1 and 2, there was no yield stress, and the sample flowed when an infinitesimally small stress was applied. COPO 3, however, displayed a yield stress of about 7 Pa, which decreased to 1 Pa as the PET block was removed (COPO 4). This indicated again that the PET block had an influence on the rheological behavior of the copolymers in aqueous solution. The existence of a yield stress after a transient suggested that the solutions contained interacting aggregates which induced an equilibrium solid-state behavior at low stress. When the stress was sufficiently high, the aggregates were reorganized, and the solutions started flowing, as it was typically observed for Bingham fluids.[28]

In a second series of experiments, the concentration of the copolymer solutions was increased up to 6%v. In Figure 2, the flow curves of COPO 2 and 3 are shown at volume fractions of 3.6% and 6% (COPO 2), and 2.4% and 3.6% (COPO 3). Similar curves to those of COPO 2 were obtained for COPO1. Two transitions were observed for COPO 1 and 2: for low concentrations (Φ < 3.6%), the solutions had a Newtonian behavior. At this concentration, the viscosity of these solutions was of the same order of magnitude as water (from 3×10^{-3} to 1×10^{-2} Pa·s depending on the concentration). At Φ = 3.6%, they showed a slightly shear-thinning behavior. At high concentrations (Φ = 6%), high stress and existence of a yield stress were observed, as shown in Figure 2a. For the COPO 3, a transition from a Newtonian behavior at Φ = 2.4% to a yielding one at Φ = 3.6% was noticed as shown in Figure 2b. With COPO 3, the transition to solutions displaying significant yield stress behavior occurred thus at lower volume fractions than with COPO 1 and 2.

At high concentration, a yield stress of about 14 and 15 Pa for COPO 1 and 2 at Φ = 6%, and about 7 Pa for COPO 3 at Φ = 3.6% was observed (Figure 2). Higher concentrations were difficult to equilibrate. Solutions of COPO 4 at high concentrations were also analyzed and have shown a transition from a shear-thinning fluid to a stress yielding one at the same concentration as for the COPO 3.

3.2. Structural Characterization by Small Angle Neutron Scattering (SANS). It was necessary to characterize the microstructure as a function of concentration to shed light on the

Table 2. Aggregates Characteristics in Solution Determined from the Guinier Approximation

	COPO 1	COPO 2	COPO 3[a]	COPO 4[a]
R_g (Å)	170	180	250	290
V_0 (Å^3)	11.6×10^6	10.2×10^6	4.8×10^6	16.7×10^6
R_0 (Å)	140	134	104	160
p	420	270	85	350

[a] Estimations of the Guinier regime.

transition from Newtonian to shear-thinning behavior and finally to a yielding fluid with concentration for the different copolymers. As a consequence, surface activity and small angle neutron scattering experiments were performed in D_2O.

Influence of Copolymer Concentration. Amphiphilic polymers usually have surface activity: in aqueous media, the copolymers form a monolayer at hydrophilic−hydrophobic interfaces. As with surfactants, tensiometry was usually used to determine the critical aggregation concentration (cac). Surface tension γ of all copolymers studied in this paper was measured at different volume fraction of polymer (Φ = 0.01% to 0.6%). For all samples, γ was constant in the concentration range studied, and its value was close to that of pure water (71.9 mN/m at 20 °C). From these measurements, it could be concluded that the studied block copolymers were surface inactive. This curious behavior was already described by Matsuoka et al.[29−31] who studied amphiphilic diblock copolymers which had polyelectrolytes as hydrophilic segment and showed no surface activity but formed micelles in water. They attributed this phenomenon to a strongly ionic nature of the hydrophilic chain. Antoun et al.[32] studied the micellization of quaternized poly(2-(dimethylamino)ethyl methacrylate)-*block*-poly(methyl methacrylate) copolymers (PDMAEMAq-*b*-PMMA) in water. They showed that when the hydrophobic block length increased, the cac was more difficult to determine because of kinetic restrictions related to decreased chain mobility. They concluded that the apparent absence of a cac might result from an exceedingly long time to reach the equilibrium conformation at the interface. In the context of dynamical properties of self-assembled aggregates, Jacquin et al.[33,34] compared diblock copolymers made of the same hydrophilic block of poly(acrylic acid) (PAA) and different hydrophobic blocks: polystyrene (PS), polybutyl acrylate (PBA) and poly(diethylene glycol ethyl ether acrylate) (PDEGA). They showed that whereas PS-*b*-PAA and PBA-*b*-PAA formed kinetically frozen aggregates in solution, PDEGA-*b*-PAA led to micelles at thermodynamic equilibrium. Their work proved that the self-assembly dynamics of amphiphilic copolymers could be controlled by the chemical nature of the insoluble block. These results were in agreement with theoretical work, which predicted that the hydrophobicity of the insoluble block was a major factor in amphiphilic copolymer self-association.[35,36]

In aqueous solutions, COPO 1 to 4 were found to form solutions with high viscosity at rather low concentrations (less than 5 wt %). This suggested that in water COPO 1 to 4 self-associated to form aggregates. With increasing concentration, interactions between the objects led to an increase of the viscosity of the solution.

To observe and understand this phenomenon, aqueous solutions of these copolymers were prepared at different volume fractions Φ ranging from 0.1 to 6% and were analyzed by SANS. In what follows, we focus on COPO 2, which is intermediate in polyelectrolyte mass between COPO 1 and 3, and then widen our observations to the other two.

Figure 3 shows the scattered intensities of aqueous solutions of COPO 2 for different volume fractions ranging from 0.1 to 6%. This figure shows that for the solutions with concentrations ranging from 0.1 to 2.4%, the intensity started from a plateau value and then decreased monotonously: it thus contained form factor information only as we will also show in the next graph. For the solutions at 3.6% (not shown for clarity, see Supporting Information) and 6%, a correlation peak appeared at q_{max} = 5.8×10^{-3} and 6.9×10^{-3} Å^{-1} (see the arrow in Figure 3), respectively. This indicated interactions between aggregates leading to a liquid-like order. We could thus distinguish the dilute regime (Φ = 0.1 to 2.4%) where independent objects were observed by SANS, from what one might call a semidilute regime (Φ = 3.6 and 6%) where correlations between objects lead to an interaction peak.

For monodisperse suspensions of spherically symmetric objects, the scattered intensity can be expressed as a product of normalized form factor $P(q)$ and structure factor $S(q)$:

$$I(q) = I_0 P(q) S(q) = \Phi V_0 \Delta\rho^2 P(q) S(q) \qquad (4)$$

where q is the magnitude of the wave vector, Φ is the aggregate volume fraction, V_0 is the dry volume of an aggregate, and $\Delta\rho$ the difference in scattering length density between the polymer and the solvent.

We applied eq 4 to the data measured in the dilute regime supposing absence of interactions, $S(q)$ = 1. The equation suggested plotting the scattered intensity normalized by the volume fraction, $I(q)/\Phi$, which was shown for dilute solutions of COPO 2 in Figure 4. The intensities were seen to superimpose nicely, apart from minor deviations at high q, which were caused by difficult background corrections. This indicated that the aggregate shape remains unchanged with the concentration, and that there were indeed no interaggregate interactions: the normalized intensity represented the form factor $P(q)$ of aggregates for solutions in the dilute regime. In this case, the scattering functions could be described by the Guinier approximation according to eq 5 within the small angle limit $q \ll 1/R_g$:

$$I(q) = I_0 \exp\left(\frac{-q^2 {R_g}^2}{3}\right) = \Phi V_0 \Delta\rho^2 \exp\left(\frac{-q^2 {R_g}^2}{3}\right) \qquad (5)$$

Equation 5 allowed us to determine the radius of gyration R_g, which gave information on the size in solution of the aggregate. The radius of gyration of COPO 2 in dilute solution was estimated as R_g = 180 Å. From I_0, the extrapolated scattered intensity at $q \to 0$, the average aggregation number (p) could be determined using the molecular volume given in Table 1 and the relationship $I_0 = V_0 \Phi \Delta\rho^2$. Aggregates of COPO 2 were found to be made of about 270 macromolecular chains (unimers). To summarize, for dilute solutions of COPO 2 (Φ < 2.4%), aggregate structure was unchanged whatever the concentration and described by R_g = 180 Å and p = 270.

Influence of Hydrophilic Block Length in the Dilute Regime. We then studied copolymers which differed from COPO 2 by their hydrophilic block length. In the dilute regime, COPO 1 and COPO 3 presented the same behavior as COPO 2: the form and the composition of the aggregates did not change with concentration as shown in the Supporting Information. As for the COPO 2, we could distinguish the dilute (Φ = 0.1 to 2.4%) from the semidilute regime (Φ = 3.6 and 6%).

Equation 5 was applied to these data and we estimated the size of the aggregates. For the COPO 3, it was unclear if the Guinier

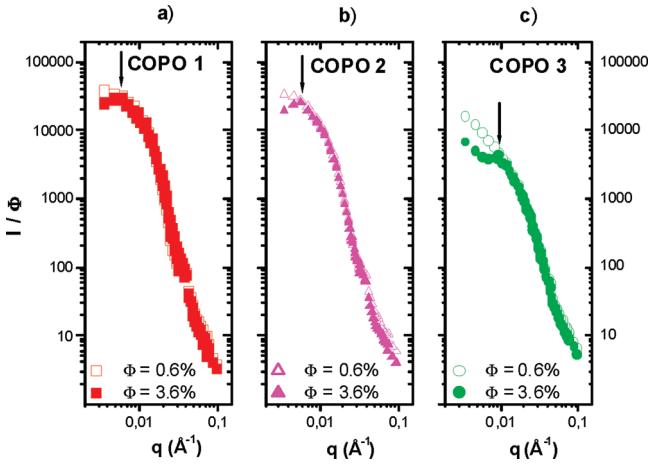

Figure 5. Comparison between COPO 1 to 3. Normalized scattered intensities are plotted at volume fractions Φ = 0.6% and 3.6% for (a) COPO1, (b) COPO 2, and (c) COPO3.

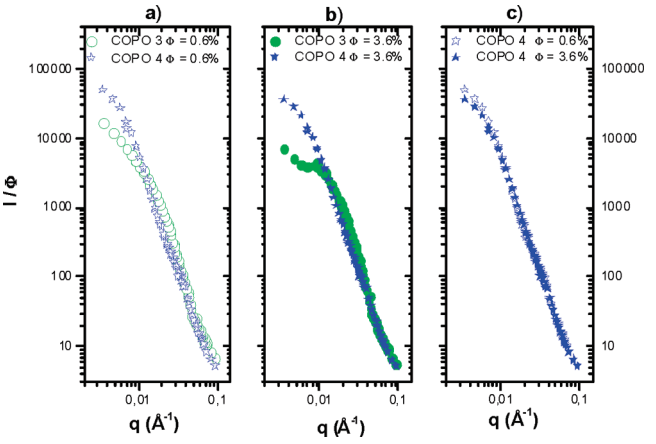

Figure 6. Scattered intensity(in cm^{-1}) normalized by the volume fraction for aqueous solutions of COPO 3 and 4. (a) COPO 3 and 4 at Φ = 0.6%, (b) COPO 3 and 4 at Φ = 3.6%, (c) COPO 4 at Φ = 0.6% and 6%.

limit was observed in our experimental q-range. Therefore, the parameters determined for COPO 3 are only estimations. The radius of gyration R_g and the aggregation number p extracted from the Guinier regime were summarized for COPO 1 to 3 in Table 2.

The radius of gyration R_g was found to increase with the hydrophilic block length. This could be easily understood: the aggregate formation in aqueous solution consisted of a hydrophobic core formed by hydrophobic segments and a charged corona/shell which ensured the solubility of aggregates in water. The increase of the hydrophilic block length induced an increase of the charged corona which led to an increase of the aggregate size. On the contrary, the aggregation number (p) decreased quickly when the hydrophilic block length went up. This might be explained by the charges of the hydrophilic block which also increase causing repulsive interactions between chains and limiting their aggregation. To summarize, with increasing polyelectrolyte block, aggregates became lighter and more swollen.

Influence of Hydrophilic Block Length in the Semidilute Regime. Figure 4 (and Supporting Information) showed that the aggregate structure did not change within the dilute regime. We then compared this structure to the one in the semidilute regime. Figure 5 represents the scattered intensity normalized by the volume fraction from aqueous solutions of COPO 1 to 3 at 0.6 and 3.6%. For a same copolymer, the scattering curves superimposed nicely at intermediate and high q. This indicated that the local aggregate structure remained unchanged when the concentration increased from 0.6% to 3.6%. A correlation peak appeared at $q_{max} = 5.8 \times 10^{-3}$ Å^{-1} for solutions at 3.6% of COPO 1 and 2 indicating interactions between aggregates. For the COPO 3, the peak appeared at the same concentration at $q_{max} = 9.2 \times 10^{-3}$ Å^{-1}.

In SANS experiments, the wave vector q_{max} provided information about the most probable distance D between aggregates which could be determined from $D = 2\pi/q_{max}$. Considering that the hydrophilic block was charged, the structure factor S(q) was due to repulsive electrostatic interactions between aggregates. Such structure factors can be described quantitatively using integral equation theories[37] and, in particular, the rescaled mean spherical approximation (RMSA) closure relation and renormalization.[38,39] Such models are rather involved and are not the scope of this article, where we have already strong evidence that the aggregate shape does not change with concentration. In the Supporting Information, a simplified modeling is presented for comparison.

Influence of the Poly(ethylene terephthalate) Block. In the triblock copolymers, the hydrophobic segment is composed of two blocks: a crystalline block, poly(ethylene terephthalate) and a rubbery one, the poly(lauryl acrylate). To analyze the influence of the crystalline block we compared aqueous solutions of COPO 4 which differs from the COPO 3 by the absence of the PET block. As previously, the form and the composition of the aggregates formed in dilute regime did not change with concentration (Supporting Information).

In Figure 6, the scattering of COPO 3 and 4 was compared for different concentrations, in the normalized presentation I/Φ. In the dilute regime (Φ = 0.6%), they did not have the same form factor. These observations suggest that form, size, and composition of aggregates were governed by two parameters: the PET block, and also (as shown before), hydrophilic block length. At higher concentration, a correlation peak appeared for the solution of COPO 3 at Φ = 3.6% indicating interactions between aggregates. On the contrary, the solution of COPO 4 at 3.6% did not present a structure peak, as shown in the comparison in Figure 6c. This might indicate that there are no interactions between the objects, or that the structure peak was outside the range of investigation. This latter point was also suggested by the intensity decrease at low q at higher concentration, and the high aggregation numbers implying large interaggregate distances, the correlation of which would be visible at small q. This last hypothesis would also be compatible with the rheological study of these solutions which showed that at 3.6% the behavior changed from a shear-thinning fluid to yielding one (Figure 1).

Average Swelling Rate of the Aggregates. From the Guinier analysis, we had information on both mass and typical spatial extension of the copolymer aggregates in solution. It appeared thus interesting to extract the evolution of the aggregate swelling with the increase of the charged hydrophilic block length. For this, we supposed aggregates were homogeneously hydrated spheres of radius R_{sp}, the Guinier relationship of which yields:

$$R_g^2 = \frac{3}{5} R_{sp}^2 \qquad (6)$$

The swelling of the aggregates could thus be estimated from the ratio of the dry volume of the aggregate $V_0 = (4\pi)/(3)R_0^3$

dx.doi.org/10.1021/ma200331b |*Macromolecules* 2011, 44, 5326–5335

Table 3. Estimation of the Equivalent Hydrated Sphere Radius and the Hydration of Aggregates in the Dilute Regime for COPO 1 to 4

	COPO 1	COPO 2	COPO 3	COPO 4
R_{sp} (Å)	220	230	320	370
$\%_{solvent}$	75	80	95	90

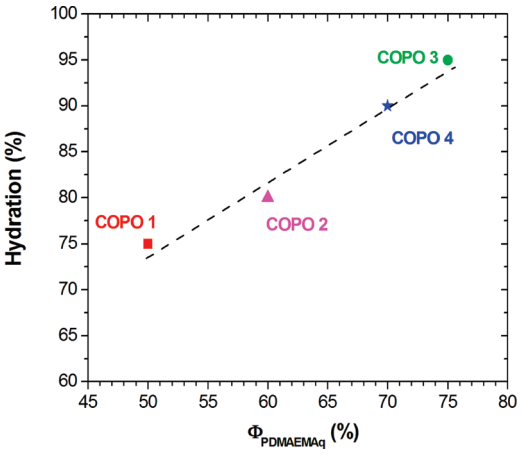

Figure 7. Swelling rate expressed as the solvent volume fraction inside aggregates as a function of the PDMAEMAq fraction in the copolymer $\Phi_{PDMAEMAq}$.

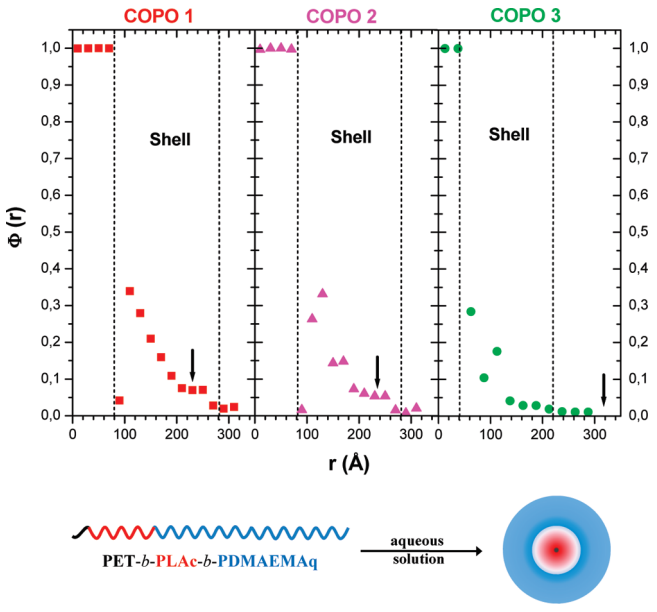

Figure 8. Radial volume fraction profile extracted from the scattering intensity for COPO 1 to 3.

and the volume of the hydrated sphere $(4\pi)/(3)R_{sp}^3$, which led to the following hydration:

$$\%_{solvent} = 1 - \left(\frac{R_0}{R_{sp}}\right)^3 \quad (7)$$

Table 3 summarizes the sphere radius and the hydration of aggregates estimated for COPO 1 to 4. Although the absolute value of this parameter remained unknown (the hydration estimated has an unknown prefactor), its relative increase with the hydrophilic block length seemed trustworthy.

We plotted the hydration as a function of PDMAEMAq fraction $\Phi_{PDMAEMAq}$ in the copolymer in Figure 7, and a linear dependence was found. By extrapolation, we have found the hydration at around 35% for $\Phi_{PDMAEMAq}$ = 0%. Even if the extrapolation was delicate, this suggested that the hydrophobic segment was also hydrated. This phenomenon was previously reported for aggregates of polymers.[22,23]

The COPO 4, which differs from the others by the absence of the PET block in the hydrophobic segment, also seemed to obey the same linear law. This suggested that PET and PLAc blocks formed the hydrophobic block which was partially hydrated.

3.3. SANS Modeling and Density Profile Determination. Up to here, we have made use only of the low-q information on the scattered intensity for a quantitative analysis. We have recently developed a model based on an "inversion" of the complete intensity curve into an average radial density profile of aggregates[24] and applied it to our data. The resulting density profiles are shown as volume fraction profiles in Figure 8, for COPO 1 to 3. The corresponding fits in reciprocal space are plotted in Figure 9.

This model described well the scattering of our copolymers in solution in the dilute regime at low and intermediate q. However, at large q, the model broke down, due to the insufficiently fine description of the density profile (finite number of points N_p). Note that a compromise has to be found between the number of points in the profile, and the amount of available information. Upon inspection of Figure 8, the aggregate core was found to be rather dry and well-defined ($\Phi(r) \approx 1$). It had the same radius for COPO 1 and 2, and was smaller for COPO 3. Although the

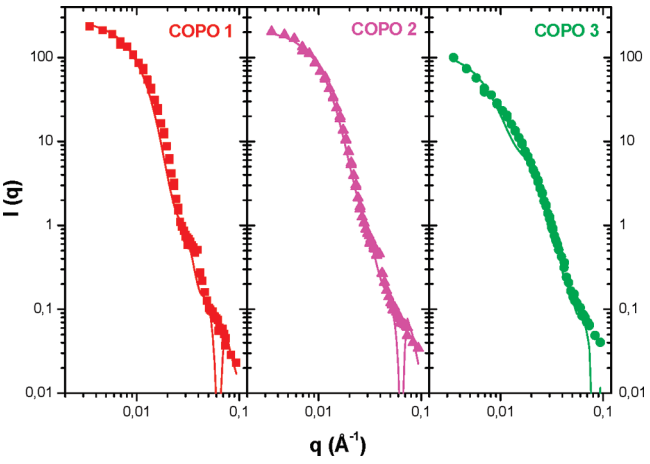

Figure 9. Fits of COPO 1 to 3 corresponding to the density profiles. Intensity is given in cm^{-1}.

Table 4. Core Radius Determined from the Density Profile and from the Aggregate Composition

	COPO 1	COPO 2	COPO 3
core radius from the density profile (Å)	80 ± 10	80 ± 10	40 ± 10
core radius for a dense PET core (Å)	40	34	23
core radius for a dense PET−PLAc core (Å)	112	96	65

Table 5. Relationship between Rheological Properties and Microstructure

	COPO 1			COPO 2			COPO 3			COPO 4		
	Φ = 2.4%	Φ = 3.6%	Φ = 6%	Φ = 2.4%	Φ = 3.6%	Φ = 6%	Φ = 2.4%	Φ = 3.6%	Φ = 6%	Φ = 2.4%	Φ = 3.6%	Φ = 6%
rheological behavior	Newt.	shear.	yield	Newt.	shear.	yield	Newt.	yield	yield	Newt.	yield	yield
structure peak	no	yes	yes	no	yes	yes	no	yes	yes	no	no	no
density parameter (%)	5.5	8	12.9	6.2	9	14.5	6.5	9.4	15.3	3.9	5.8	9.4

general tendency of the aggregation number was a decrease with increasing polyelectrolyte block (Table 2), the evolution of the core volume was not directly related to the aggregation number. Indeed, the size of the core could be compared to the dry size of a pure dense PET core, or a core made of both PET and PLAc, as shown in Table 4. It was seen that the aggregate core could not contain all the hydrophobes, and that some the hydrophobic segments were hydrated in the aggregate shell. In each volume fraction profile, the shell volume fraction was to seen to decrease from about 30% down to zero. This was in line with the observation in Figure 7 of a nonzero hydration when extrapolating our data to very small polyelectrolyte blocks.

The spatial extension of the hydrated shell could be read off from the profiles (Figure 8). It was about the same (200 Å) for COPO 1 and 2. The situation was less clear for COPO 3, where the highly hydrated shell extended up to very high radii. This was compatible, e.g., with the high radius of gyration. The densest part of the shell, proved to be smaller, ca. 180 Å, for COPO 3.

4. DISCUSSION

We attempted to rationalize the results on the microstructure and the rheological properties of the copolymer solutions. The structure of the copolymer aggregates could be analyzed at low concentrations: the radius of gyration and the aggregation number has been measured for COPO 1 and 2, and estimated with reasonable accuracy for the other two. The aggregation number showed a strong dependence on the mass of the polyelectrolyte block, decreasing by almost a factor of 2 from COPO 1 to 2, then again by a factor of 3. By superimposing the scattered intensity of low and high concentrations ($\Phi > 2.4\%$) in the normalized presentation I/Φ, we could show that the local structure of the aggregates remained unchanged. Plotting the aggregation number p as a function of the polymerization degree of the polyelectrolyte block PD showed that p followed a power law ($p \approx \mathrm{PD}^{-1.4}$). The exponent could be compared to predictions of theories for weakly and strongly charged chains,[40,41] which found exponents varying between 1 and 3.

Finally, the copolymer without PET had also a very high aggregation number. This illustrated the strong influence of the PET block on the structure, and concomitantly, on the rheology. Indeed, the radius of gyration increased, and simultaneously, the aggregation number increased much more, leading to less space filling aggregates having a lower degree of hydration. In the semidilute regime, traces of the interaction between the big aggregates were visible from the very small angle scattering, but the scattering peak (if it exists) was outside the q-range of investigation.

The internal structure of the aggregates was studied using both a simple estimation of their average hydration, and a more elaborate model based on an "inversion" of the scattering data into a volume fraction profile $\Phi(r)$. As a cross-check, the radii of gyration could be estimated from the profile:

$$R_g^2 = \frac{\int \Phi(r) \cdot r^4 \, dr}{\int \Phi(r) \cdot r^2 \, dr} \tag{8}$$

The values for COPO 1 and 2 ($R_g = 182 \pm 10$ Å and 173 ± 10 Å, respectively) were in good agreement with those determined with the Guinier-analysis, (Table 2). For COPO 3, the agreement was also good ($R_g = 243 \pm 10$ Å). However, it was observed that $\Phi(r)$ did not tend to zero quickly enough in the r-range of investigation, and shells of very low density located at rather large r still contributed significantly to the integral in eq 8. It would be straightforward to model the high-r data, but lower q-values would be needed. For the q-range measured here, it could be concluded that most of the monomers of COPO 3 were captured by the volume fraction profile given in Figure 8, with a more extended low-density shell existing at $r > 300$ Å.

The hydration was estimated from the equivalent homogeneous sphere radius. It showed a surprising linear law in polyelectrolyte mass, which could be extrapolated to suggest considerable hydration of a hypothetical polyelectrolyte-free aggregate (i.e., consisting only of a hydrophobic core). This finding was backed up by the volume fraction profiles. The latter always displayed a solvent-free core of 80−40 Å radius, followed by a small shell containing solvent and about 20−30% of polymer. From a geometric estimation of the available volumes of monomers, it could be concluded that the core was probably made of PET and some PLAc, the rest of the PLAc being hydrated in the shell surrounding the core. The polyelectrolyte, finally, occupied an outer shell of even lower density. The estimation of the hydration using eq 7, which had an unknown prefactor, could be compared to the volume fraction profiles by locating the equivalent homogeneous sphere radius R_{sp} by the arrows in Figure 8. It was concluded from the low values of the volume fraction profiles at R_{sp} that the unknown prefactor for eq 7 was close to one, and our estimation of hydration trustworthy.

We tried to relate the rheology of the studied system to the microstructure. It appeared that the volume spanning properties of the hydrated aggregates had to be of primary importance to the transition from a liquid to a solid state. We have therefore defined a parameter expressing the degree of occupation of available volume by an average aggregate:

$$v = \Phi \times \frac{(R_{tot} + \lambda_D)^3}{\frac{4\pi}{3} R_0^3} \tag{9}$$

where Φ is the aggregate volume fraction, R_{tot} the radius of the aggregate determined from the density profile in agreement with the dense shell thickness (280, 280, and 220 Å, for COPO 1, 2, and 3, respectively), λ_D the Debye length (which characterizes the electrostatic range of interaction), and R_0 the dry radius of the

aggregate. Note that this parameter v reflects both the hydration and volume fraction of matter in the sample.

Table 5 links the rheological behavior of each copolymer studied to the microstructure of the aggregates and the concentration. If one excludes the only diblock copolymer, COPO 4, from the discussion, it was found that a limiting value of least 6.5 for the density parameter could be found: all samples with density parameters below this value showed Newtonian behavior. The sample without the PET-block, COPO 4, displayed yielding already at 3.6%, with a density parameter of 5.8. This might be due to the influence of the glassy state of PET, as its presence induced an increase of stress leading to the formation of frozen micelles. Although the PET-block was quite short, apparently its glassy dynamics ($T_{g,PET}$ = 80 °C) affected the reorganization dynamics of the micelles. Then, the morphology and structure of frozen micelles depended on sample preparation.[42,43] Copolymer micelles without PET had a liquid-like core at room temperature ($T_{g,PLAc}$ = −3 °C) which, in principle, favored unimer exchange and micellar reorganization.

5. CONCLUSION

We have investigated the structure of a series of poly(ethylene terephthalate)-*b*-poly(lauryl acrylate)-*b*- quaternized poly(2-(dimethylamino)ethyl methacrylate), or PET-*b*-PLAc-*b*-PDMAEMAq triblock copolymers in aqueous solutions differing from the polyelectrolyte block molecular weight (and the absence of PET for one). The rheological nature of these solutions changed with concentration, and a nonzero yield stress was found at rather low concentrations (below typically 5%). This was put in parallel with interactions visible in scattering between copolymer aggregates in solution, resulting from their increasingly space-filling properties as the polyelectrolyte block grew. The rheological behavior of solutions of these amphiphilic copolymers was investigated using dynamic and creep experiments. We observed that the rheological nature of the solutions changed with concentration from a Newtonian flow at low concentrations, to a shear-thinning one at intermediate concentrations, and finally to a yield behavior at large concentrations. The PET block had a strong influence on the rheology and on the aggregate microstructure. SANS experiments and density profile showed that PET-*b*-PLAc-*b*-PDMAEMAq triblock copolymers formed frozen aggregates in aqueous solutions composed of a solvent-free core made of PET and some PLAc, followed by a small shell containing of the rest of PLAc which was hydrated and finally an outer shell of the hydrated polyelectrolyte. The aggregation number p presented dependence over the polyelectrolyte mass.

■ ASSOCIATED CONTENT

Ⓢ Supporting Information. Experimental procedures, scattering data, modeling of the structure factor peak, and rheology. This material is available free of charge via the Internet at http://pubs.acs.org.

■ AUTHOR INFORMATION

Corresponding Author

*(J.O.) Telephone: 33-4-67-14-35-23. Fax: 33-4-67-14-34-98. E-mail: Julian.Oberdisse@univ-montp2.fr. (S.M.) Telephone: 33-4-67-14-41-58. Fax: 33-4-67-14-40-28. E-mail: Sophie.Monge-Darcos@univ-montp2.fr.

■ ACKNOWLEDGMENT

We thank the French Environment and Energy Management Agency (ADEME) and the Region Languedoc-Roussillon for financial support. We are also grateful to Fabrice Cousin and Jacques Jestin from LLB, France for help with SANS experiments.

■ REFERENCES

(1) Fairley, N.; Hoang, B.; Allen, C. *Biomacromolecules* **2008**, *9*, 2283–2291.
(2) Habas, J.-P.; Pavie, E.; Lapp, A.; Peyrelasse, J. *Rheol. Acta* **2008**, *47*, 765–776.
(3) Mortensen, K.; Pedersen, J. S. *Macromolecules* **2002**, *26*, 805–812.
(4) Perreur, C.; Habas, J.-P.; Peyrelasse, J.; Francois, J.; Lapp, A. *Phys. Rev. E: Stat., Nonlinear, Soft Matter Phys.* **2001**, *63*, 031505/1–031505/11.
(5) Price, E. W.; Guo, Y.; Wang, C. W.; Moffitt, M. G. *Langmuir* **2009**, *25*, 6398–6406.
(6) Reinicke, S.; Schmelz, J.; Lapp, A.; Karg, M.; Hellweg, T.; Schmalz, H. *Soft Matter* **2009**, *5*, 2648–2657.
(7) Baines, F. L.; Billingham, N. C.; Armes, S. P. *Macromolecules* **1996**, *29*, 3416–20.
(8) Fang, Z.; Wang, S.; Wang, S. Q.; Kennedy, J. P. *J. Appl. Polym. Sci.* **2003**, *88*, 1516–1525.
(9) Lee, A. S.; Buetuen, V.; Vamvakaki, M.; Armes, S. P.; Pople, J. A.; Gast, A. P. *Macromolecules* **2002**, *35*, 8540–8551.
(10) Petrov, P.; Tsvetanov, C. B.; Jerome, R. *Polym. Int.* **2008**, *57*, 1258–1264.
(11) Kellum, M. G.; Smith, A. E.; York, S. K.; McCormick, C. L. *Macromolecules* **2010**, *43*, 7033–7040.
(12) Testard, V.; Oberdisse, J.; Ligoure, C. *Macromolecules* **2008**, *41*, 7219–7226.
(13) Rufier, C.; Collet, A.; Viguier, M.; Oberdisse, J.; Mora, S. *Macromolecules* **2009**, *42*, 5226–5235.
(14) Colomines, G.; Robin, J.-J.; Tersac, G. *Polymer* **2005**, *46*, 3230–3247.
(15) Colomines, G.; Lee, A. V. D.; Robin, J.-J.; Boutevin, B. *Macromol. Chem. Phys.* **2006**, *207*, 1461–1473.
(16) Rufier, C.; Collet, A.; Viguier, M.; Oberdisse, J.; Mora, S. *Macromolecules* **2008**, *41*, 5854–5862.
(17) Liénafa, L.; Monge, S.; Robin, J.-J. *Eur. Polym. J.* **2009**, *45*, 1845–1850.
(18) Narrainen, A. P.; Pascual, S.; Haddleton, D. M. *J. Polym. Sci., Part A: Polym. Chem.* **2002**, *40*, 439–450.
(19) Liénafa, L.; Monge, S.; Robin, J.-J. To be published.
(20) Sears, V. F. *Neutron News* **1992**, *3*, 26–37.
(21) Ribaut, T.; Oberdisse, J.; Annighofer, B.; Stoychev, I.; Fournel, B.; Sarrade, S.; Lacroix-Desmazes, P. *Soft Matter* **2009**, *5*, 4962–4970.
(22) Sotiropoulou, M.; Bossard, F.; Balnois, E.; Oberdisse, J.; Staikos, G. *Langmuir* **2007**, *23*, 11252–11258.
(23) Sotiropoulou, M.; Oberdisse, J.; Staikos, G. *Macromolecules* **2006**, *39*, 3065–3070.
(24) Ribaut, T.; Oberdisse, J.; Annighofer, B.; Fournel, B.; Sarrade, S.; Haller, H.; Lacroix-Desmazes, P. *J. Phys. Chem. B* **2011**, *115*, 836–843.
(25) Glatter, O. *J. Appl. Crystallogr.* **1977**, *10*, 415–421.
(26) Oberdisse, J.; Hine, P.; Pyckhout-Hintzen, W. *Soft Matter* **2007**, *3*, 476–485.
(27) Puech, N.; Mora, S.; Phou, T.; Porte, G.; Jestin, J.; Oberdisse, J. *Soft Matter* **2010**, *6*, 5605–5614.
(28) Bauer, T.; Oberdisse, J.; Ramos, L. *Phys. Rev. Lett.* **2006**, *97*, 258303.
(29) Kaewsaiha, P.; Matsumoto, K.; Matsuoka, H. *Langmuir* **2005**, *21*, 9938–9945.
(30) Matsuoka, H.; Maeda, S. i.; Kaewsaiha, P.; Matsumoto, K. *Langmuir* **2004**, *20*, 7412–7421.
(31) Matsuoka, H.; Matsutani, M.; Mouri, E.; Matsumoto, K. *Macromolecules* **2003**, *36*, 5321–5330.

(32) Antoun, S.; Gohy, J. F.; Jerome, R. *Polymer* **2001**, *42*, 3641–3648.
(33) Jacquin, M.; Muller, P.; Cottet, H.; Théodoly, O. *Langmuir* **2010**, *26*, 18681–18693.
(34) Jacquin, M.; Muller, P.; Talingting-Pabalan, R.; Cottet, H.; Berret, J. F.; Futterer, T.; Théodoly, O. *J. Colloid Interface Sci.* **2007**, *316*, 897–911.
(35) Haliloglu, T.; Bahar, I.; Erman, B.; Mattice, W. L. *Macromolecules* **1996**, *29*, 4764–4771.
(36) Nose, T.; Iyama, K. *Comput. Theor. Polym. Sci.* **2000**, *10*, 249–257.
(37) Hansen, J. P.; McDonald, I. R. *Theory of Simple Liquids*; Academic Press: London, 1986.
(38) Hayter, J. B.; Penfold, J. *Mol. Phys.* **1981**, *42*, 109–118.
(39) Hansen, J. P.; Hayter, J. B. *Mol. Phys.* **1982**, *46*, 651–656.
(40) Halperin, A. *Polym. Rev.* **2006**, *46*, 173–214.
(41) Marko, J. F.; Rabin, Y. *Macromolecules* **1992**, *25*, 1503–1509.
(42) Selb, J.; Gallot, Y. *Developments in Block Copolymers*; 2nd ed.; Elsevier: Amsterdam, 1985.
(43) Yu, Y.; Zhang, L.; Eisenberg, A. *Macromolecules* **1998**, *31*, 1144–1154.